

# Advanced in situ and laboratory characterisation of the ALPACA chalk research site

KEN VINCK<sup>\*</sup>, TINGFA LIU<sup>†</sup>, RICHARD J. JARDINE<sup>‡</sup>, STAVROULA KONTOE<sup>§</sup>,  
REZA AHMADI-NAGHADEH<sup>||</sup>, RÓISÍN M. BUCKLEY<sup>¶</sup>, BYRON W. BYRNE<sup>\*\*</sup>,  
JAMES A. LAWRENCE<sup>††</sup>, ROSS A. MCADAM<sup>‡‡</sup> and FABIAN SCHRANZ<sup>§§</sup>

Low- to medium-density chalk at St Nicholas at Wade, UK, is characterised by intensive testing to inform the interpretation of axial and lateral tests on driven piles. The chalk destructures when taken to large strains, especially under dynamic loading, leading to remarkably high pore pressures beneath penetrating cone penetration testing and driven pile tips, weak putty annuli around their shafts and degraded responses in full-displacement pressure-meter tests. Laboratory tests on carefully formed specimens explore the chalk's unstable structure and markedly time- and rate-dependent mechanical behaviour. A clear hierarchy is found between profiles of peak strength with depth of Brazilian tension, drained and undrained triaxial and direct simple shear tests conducted from in situ stress conditions. Highly instrumented triaxial tests reveal the chalk's unusual effective stress paths, markedly brittle failure behaviour from small strains and the effects of consolidating to higher than in situ stresses. The chalk's mainly sub-vertical jointing and micro-fissuring lead to properties depending on specimen scale, with in situ mass stiffnesses falling significantly below high-quality laboratory measurements and vertical Young's moduli exceeding horizontal stiffnesses. While compressive strength and stiffness appear relatively insensitive to effective stress levels, consolidation to higher pressures closes micro-fissures, increases stiffness and reduces anisotropy.

**KEYWORDS:** chalk; full-scale pile testing; in situ testing; laboratory testing; piles & piling; site investigation

## INTRODUCTION

Recent offshore North and Baltic Sea wind energy-generating projects have demonstrated that current recommendations are insufficiently reliable to guide safe and economical driven pile design in chalk, a very weak to weak biomicrite limestone. Considerable uncertainty exists regarding driving resistances, axial capacities at a range of ages and

response to lateral and cyclic loading; Barbosa *et al.* (2015, 2017), Muir Wood *et al.* (2015), Carotenuto *et al.* (2018), Jardine *et al.* (2018) and Buckley *et al.* (2020a).

The ALPACA (axial-lateral pile analysis for chalk applying multi-scale field and laboratory testing) and ALPACA Plus joint industry projects (JIPs) described by Jardine *et al.* (2019) and Buckley *et al.* (2020b) addressed these shortcomings by conducting multiple large-scale field experiments on piles driven at the St Nicholas-at-Wade (SNW) test site in the UK. This paper describes intensive characterisation research conducted to aid the pile experiments' interpretation. It also provides new insights for other geotechnical problems involving chalk.

Manuscript received 13 July 2021; revised manuscript accepted 19 January 2022.

Discussion on this paper is welcomed by the editor.

Published with permission by the ICE under the CC-BY 4.0 license. (<http://creativecommons.org/licenses/by/4.0/>)

<sup>\*</sup> Department of Civil and Environmental Engineering, Imperial College London, London, UK (Orcid:0000-0002-0990-0895).

<sup>†</sup> Department of Civil Engineering, University of Bristol, Bristol, UK; formerly Department of Civil and Environmental Engineering, Imperial College London, London, UK

(Orcid:0000-0002-5719-8420).

<sup>‡</sup> Department of Civil and Environmental Engineering, Imperial College London, London, UK (Orcid:0000-0001-7147-5909).

<sup>§</sup> Department of Civil and Environmental Engineering, Imperial College London, London, UK (Orcid:0000-0002-8354-8762).

<sup>||</sup> Formerly Department of Civil and Environmental Engineering, Imperial College London, London, UK; now Department of Construction Engineering and Lighting Science, School of Engineering, Jönköping University, Jönköping, Sweden (Orcid:0000-0002-2215-441X).

<sup>¶</sup> School of Engineering, Glasgow, UK

(Orcid:0000-0001-5152-7759).

<sup>\*\*</sup> Department of Engineering Science, Oxford University, Oxford, UK (Orcid:0000-0002-9704-0767).

<sup>††</sup> Department of Civil and Environmental Engineering, Imperial College London, London, UK (Orcid:0000-0002-9781-817X).

<sup>‡‡</sup> Department of Engineering Science, Oxford University, Oxford, UK (Orcid:0000-0003-0292-3549).

<sup>§§</sup> Office of the Tyrolean Regional Government, Innsbruck, Austria.

## STUDY AIMS AND BACKGROUND

The aims of the study were to

- enable analyses of the field experiments by investigating the chalk comprehensively through advanced in situ and laboratory techniques
- establish how chalk's structure, pore pressures and mechanical properties vary from ground level to the maximum pile tip depth (20 m)
- investigate the influences of applied stress path, pressure and strain levels, principal stress axis orientation and strain rates on the chalk's mechanical behaviour.

Chalk's sedimentary and cementing-in-place processes allow low- to medium-density formations to retain in situ liquidity indices close to unity, even after deep burial (Mortimore, 2012). Variable density profiles are common, as is parallel-to-bedding anisotropy (Hickman, 2004). Hard silica flint bands are also often encountered. Upper Cretaceous syn-sedimentary and subsequent depositional processes related to burial and tectonics, combined with more

recent Quaternary periglacial action and weathering, led to fractured rock showing multiple types of discontinuities at a range of scales. The Ciria (Lord *et al.*, 2002) classification scheme therefore considers, in addition to intact dry density (IDD), differences between natural and induced fractures and deterioration within chalk blocks, and structure.

Locally instrumented triaxial tests involving routine confining pressures indicate stiff and near-elastic initial behaviour in single unfractured elements, with yielding at axial strains < 0.15%, followed by brittle failure, dilation and fracturing (Jardine *et al.*, 1984, 1985). Stiffness may be significantly anisotropic (Talesnick *et al.*, 2001; Korsnes *et al.*, 2008). Natural micro- to macro-fissuring reduces mass stiffness in situ, particularly in high-density chalks (Matthews & Clayton, 1993; Clayton *et al.*, 1994, 2002; Holloway-Strong *et al.*, 2007). High-pressure compression tests reveal ‘pore collapse’ (Collin *et al.*, 2002) when the chalk ‘destructures’ (Leroueil & Vaughan, 1990) as bonds break and both hollow calm carbonate (CaCO<sub>3</sub>) particles and macro-void spaces collapse (Petley *et al.*, 1993). The chalk’s post-yield behaviour is also time and strain rate dependent (Addis & Jones, 1990; Leddra *et al.*, 1993; Bialowas, 2017). De Gennaro *et al.* (2004) and Ma *et al.* (2019) discuss fundamental aspects of how chalk properties vary with physiochemical changes within its pore space.

Deconstructed reconstituted chalk has been studied by Clayton (1977), Razoaki (2000), Bundy (2013), Alvarez-Borges (2019) and Bialowas (2017). Dynamic percussion, cone penetration test (CPT) penetration and pile driving in high-porosity chalks produce putties, whose shear strengths are compatible with their liquidity indices, but which gain strength and stiffness when allowed to reconsolidate, creep and age (Doughty *et al.*, 2018). Shear strengths < 20 kPa have been noted in thin annuli formed around piles shortly after driving (Hobbs & Atkinson, 1993; Lord *et al.*, 2002; Buckley *et al.*, 2018). Cyclic CPT probing can reduce friction sleeve resistances to  $\approx 4$  kPa (Diambra *et al.*, 2014). High-amplitude, displacement-controlled simple shear cycling produces comparably weak putties (Carrington *et al.*, 2011).

The above studies helped define the ALPACA characterisation agenda. Earlier investigations at SNW concentrated on sampling trials, piezocone testing (CPT with pore pressure measurement (CPTu)) and geophysics, with relatively sparse laboratory testing (Buckley *et al.*, 2018). The ALPACA field work included, as identified in Fig. 1, multiple new

soundings, pressuremeter profiling, three boreholes and a large sampling excavation after pile testing. The comprehensive laboratory programme included index and oedometer profiling and over 100 advanced tests with locally instrumented, automated, stress path triaxial equipment. This paper summarises the central findings. Additional high-pressure (up to 13 MPa) laboratory tests are reported separately by the ALPACA Academic Working Group (ALPACA AWG, 2022), while Ahmadi-Naghadeh *et al.* (2022) explore the intact chalk’s cyclic loading response and Liu *et al.* (2022) consider the monotonic and cyclic behaviour of putified chalk reconsolidated to stresses comparable to those acting around the pile shafts.

## FIELD CHARACTERISATION

The site occupies a former quarry at UK grid: TR 25419 66879, near Margate in Kent. Up to 5 m of excavation took place before sampling and geophysical trials with compression (P) and shear (S) wave (PS) logging, cross-hole and down-hole seismic testing by SETech (2007). Investigations for the ‘Wind-support’ and ‘Innovate UK’ pile test programmes (Ciavaglia *et al.*, 2017a, 2017b; Buckley *et al.*, 2018, respectively) concentrated on CPTu and seismic CPT (SCPT) profiling.

The ALPACA investigations located the water table  $\approx 0.9$  m above ordnance datum (AOD), with  $\pm 0.25$  m variations and found < 0.5 ppt sodium chloride (NaCl) in the groundwater. A tensiometer installed at 3 m depth indicated seasonally varying suctions around 30 kPa. CPTu or SCPT soundings were made for each of the 41 test piles shown in Fig. 1. Cone pressure-meter testing was conducted and samples from three 16 m deep, Geobore-S wireline rotary boreholes were cleaned, partitioned, sealed and preserved immediately on-site. Eighteen 350 × 350 × 250 mm blocks were sampled from a 7 m × 10 m, 4 m deep, excavation. Careful hand sampling mobilised, wherever possible, pre-existing fissures and (mainly horizontal) bedding planes to minimise disturbance; all visibly fractured material was avoided. Hand and chainsaws were used to disconnect blocks which were preserved immediately in successive layers of foil, cling-film and wax. Expanding polyurethane foam secured the blocks in plywood storage boxes.

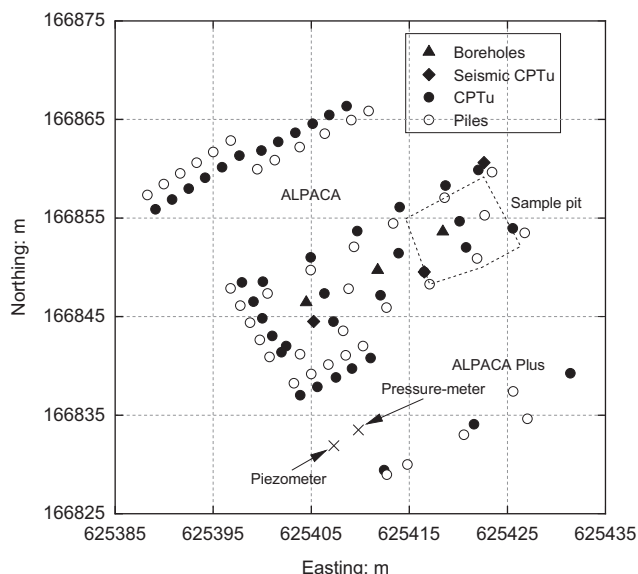


**Fig. 1. Plan layout of ALPACA and ALPACA Plus pile and ground characterisation locations**

### Stratigraphy and structure

Vinck (2021) details the chalk’s stratigraphy and structure, noting pure (98.6% calm carbonate (Hancock, 1975)) white Margate Chalk, showing slight weathering near ground level, occasional small flints and very few macrofossils, extending down to the yellow iron-stained Barrois’ Sponge Bed at 5.2 m AOD, which marks the unit’s base and contains echinoid *Micraster* fossils. Below this is horizontally bedded Seaford Chalk, with regular discontinuous nodular flint bands, including ‘Whitaker’s three-inch’ flint marker at  $-7.5$  m AOD.

The chalk classifies as Ciria Grade B3/B2 (structured, very weak to weak, low to medium density) over the depths of interest, with discontinuity apertures < 3 mm and fractures spaced at 60 to 600 mm. The fractures become tighter from  $-2.7$  m AOD as the Grade improves to A2. Predominantly vertical linear features and micro-fissures were identified at all depths with  $\approx 10$  to 25 mm spacings as described by Lawrence *et al.* (2018). The excavation pit revealed that pile driving, lateral testing and excavating opened discontinuities and reduced the upper chalk to Grade C.

INDEX AND IN SITU TESTING

Index properties

Chalk particle size analyses are affected by particle fracture and testing methodology (Clayton *et al.*, 2002). However, both manually ground-down dried SNW chalk, and putty formed by compaction at natural water content present as fine silts with  $D_{50}$  around 3–4  $\mu\text{m}$  in hydrometer and laser diffraction analyses. The index properties summarised in Fig. 2 and Table 1 indicate low-density chalk (Mortimore, 2012), with 1.43 to 1.53  $\text{Mg/m}^3$  intact dry densities and a 0.91 average liquidity index. The degree of saturation  $S_r$  increases from  $\approx 0.85$  near the ground surface to  $\approx 0.97$  just above the water table and  $\approx 1.00$  below.

Cone penetration tests

Figure 3 presents typical CPTu and SCPT profiles. Corrected ( $q_t$ ) resistances range from around 5 to 35 MPa, with higher resistances in thin, discrete, often discontinuous flint bands. Destructuration starts beneath the tips and excess pore pressures as high as 10 MPa were measured at  $u_1$  (face) piezocone positions (Buckley, 2018), while lower, but still remarkably high, pressures develop at  $u_2$  (shoulder) locations. Friction sleeve resistances of 0.05 to 1 MPa persist as the chalk flows past. Forty-eight CPTu dissipation tests showed 50% equalisation times,  $t_{50}$ , <10 s in most cases, indicating  $7 \times 10^4 \text{ m}^2/\text{year}$  ( $\pm 35\%$ ) radial coefficients of consolidation,  $c_{h,\text{piezo}}$  when the chalk's high rigidity index is recognised.

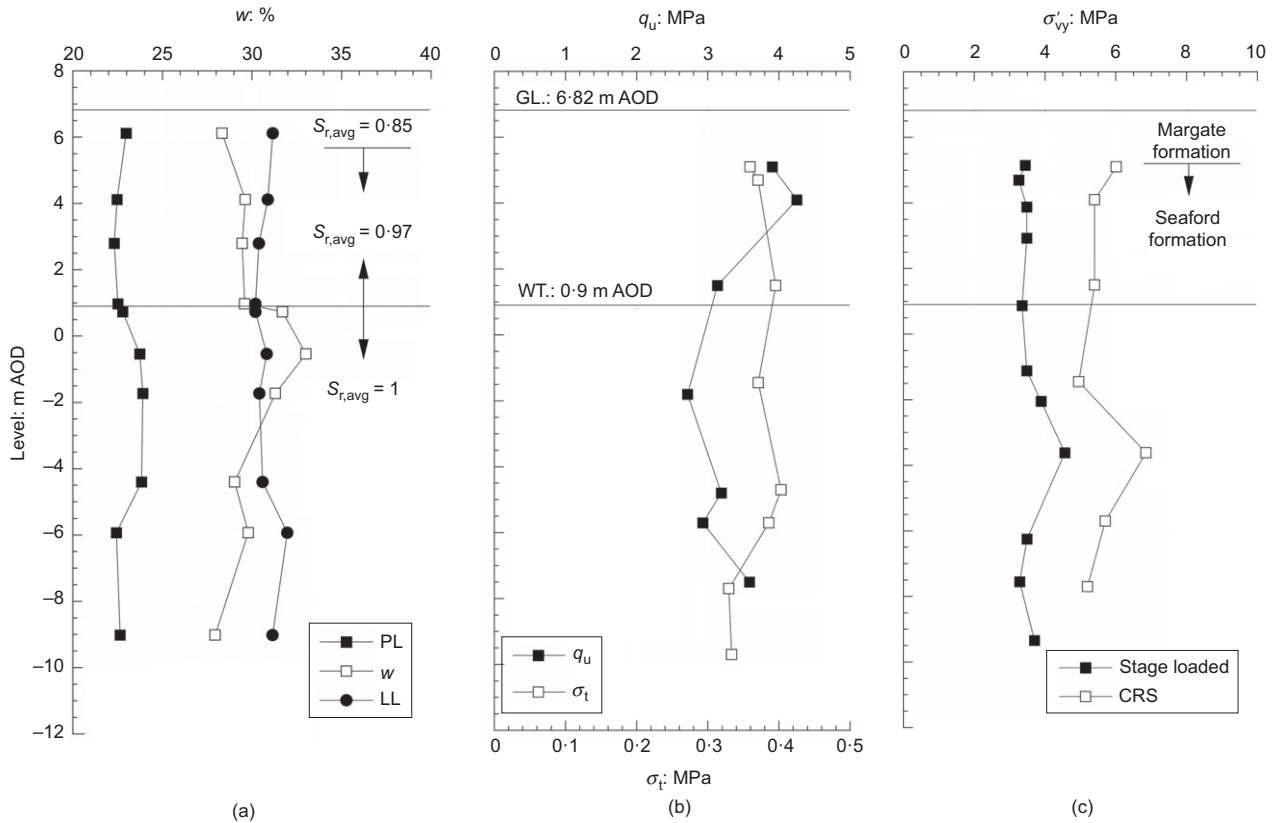


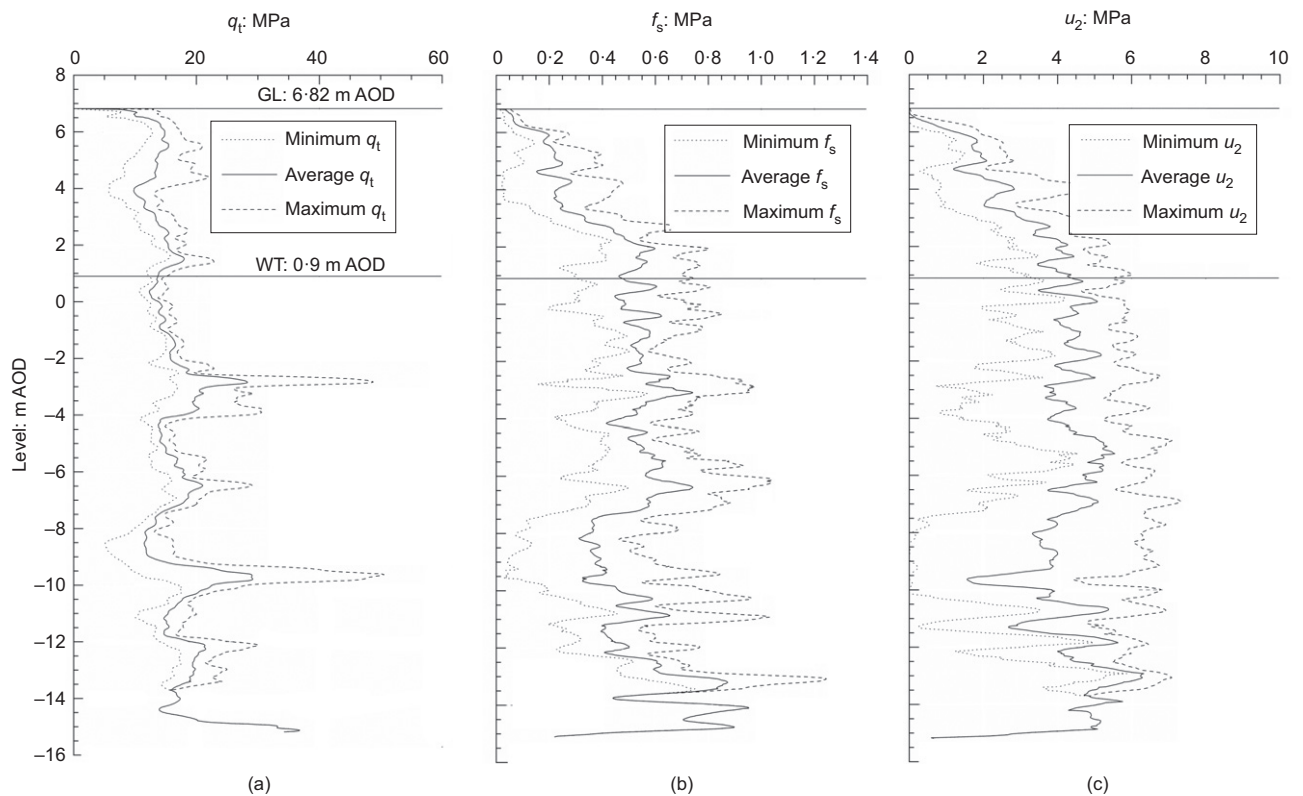
Fig. 2. Profiles for SNWALPACA site of (a) natural water content and Atterberg limits; (b) UCS and BT strengths; (c)  $\sigma_{vy}$  values from stage loaded oedometer and CRS tests; ground level (GL), water table (WT) depth and stratigraphy also shown

Table 1. Typical index properties of chalk samples

Depth: m BGL	Level: AOD	$\rho_b$ : $\text{g/cm}^3$	$\rho_d$ : $\text{g/cm}^3$	w: %	LL: %	PI: %	$S_r^*$	$n^\dagger$
0.70	6.52	1.85	1.44	28.33	31.16	8.19	0.87	46.8
2.70	4.52	1.91	1.47	29.63	30.88	8.41	0.96	45.6
4.03	3.20	1.93	1.49	29.45	30.39	8.08	0.98	45.0
5.85	0.97	1.91	1.47	29.59	30.20	7.68	0.96	45.6
6.09	0.83	1.89	1.44	31.71	30.19	7.41	0.97	47.0
7.36	-0.44	1.90	1.43	33.01	30.82	7.08	1.00	47.2
8.55	-1.63	1.91	1.45	31.30	30.41	6.50	0.98	46.3
11.22	-4.30	1.98	1.53	29.03	30.59	6.76	1.00	43.4
12.75	-5.83	1.92	1.48	29.80	31.97	9.54	0.97	45.5
15.84	-8.92	1.92	1.50	27.94	31.15	8.51	0.94	44.5
Min.		1.85	1.43	27.94	30.19	6.50	0.87	43.4
Max.		1.98	1.53	33.01	31.97	9.54	1.00	47.2
Avg.		1.91	1.47	29.98	30.78	7.82	0.96	45.7
St. Dev.		0.03	0.03	1.57	0.55	0.92	0.04	1.18

\*Based on a measured specific gravity,  $G_s = 2.71$ .

$^\dagger n$  is porosity.



**Fig. 3. Summary of piezocone profiles from ALPACA Plus JIP at SNW site**

Vinck (2021) estimates  $5 \times 10^{-9}$  to  $7 \times 10^{-8}$  m/s permeabilities (depending on bulk stiffness estimates) from these inevitably ‘disturbed’ in situ experiments, while laboratory tests on southern Seaford chalk show mid-range  $k_v$ ,  $\approx 2 \times 10^{-8}$  m/s (Marley, 2020). The chalk’s open fractures do not constrain the disturbed CPTu or ‘small volume’ laboratory measurements but lead to higher undisturbed mass permeability in situ. Simplified consolidation analyses indicate that CPT penetration may be partially drained at SNW (Buckley *et al.*, 2018).

In situ shear wave velocities measured at SNW generally fall below the  $1.0 \text{ km/s} < V_s < 1.8 \text{ km/s}$  range of Røgen *et al.* (2005) for low- to medium-density North Sea chalk. Fig. 4 illustrates shear moduli from cross-hole and PS logging (SETech, 2007; Fugro, 2012), along with ALPACA project SCPTs.

#### Pressure-meter tests

Pressure-meter testing has been employed to aid offshore wind turbine foundation design in chalk (Whittle *et al.*, 2017). Cambridge Insitu Ltd undertook and interpreted testing with a 47 mm dia., 0.5 m long cone push-in pressure-meter inserted into cavities formed by CPT probing. Initial inflations to around 2 mm radial displacement took place over 15 to 20 min, including two unload–reload loops. Further loops were imposed during deflation, as shown in Fig. 5. Test analysis poses multiple challenges as consistent interpretation methodologies have yet to be developed specifically for chinks (Whittle *et al.*, 2017). Homogeneous, continuously non-linear, elastic shear stiffnesses were assumed, after Bolton & Whittle (1999), which varied in proportion to  $p'$  raised to an exponent  $n$ , while Poisson’s ratio  $\nu' = 0.2$ . Iterative hindcasts applying Withers *et al.* (1989) drained plane-strain analysis, assuming non-associated Mohr–Coulomb yielding and  $c' = 0$  indicated

best-fitting  $\phi'$  values of  $31^\circ \pm 5^\circ$ , dilation angles  $\psi$  of  $0^\circ$  to  $-12^\circ$ , suggesting volumetric contraction. Exponent  $n$  increased with depth from 0.4 to 0.63 and Fig. 5 shows the non-linear (implicitly  $G_{hh}$  mode) shear moduli scaled to in situ  $p'$  for each depth. It is difficult to resolve very-small-strain stiffnesses from pressure-meter tests and the curves plotted in Fig. 5 start from the  $\gamma_{min} = 0.01\%$  limit at which reliable measurements could be made, which appears to exceed any linear range. The maximum  $G_{hh}$  values grow from 148 MPa to 231 MPa with depth and represent  $\approx 20\%$  of the elastic geophysical  $G_{hh}$  trends in Fig. 4. The curves reflect the non-linear properties of partially destructured chalk, which plays a role in defining the behaviour of open-steel piles driven in chalk (Lord *et al.*, 2002).

## MECHANICAL LABORATORY TESTS

### Laboratory specimen preparation

Laboratory mechanical test specimens require very careful preparation in chalk (Jardine *et al.*, 1984, 1985). Trials revealed a need for plaster-of-Paris confining moulds and water-flush coring with a highly stable radial-arm drill. The resulting cores were enclosed in split aluminium moulds and machined to achieve ASTM (2019) end flatness and parallelism tolerances.

### Unconfined compression (UCS), Brazilian tension (BT) and oedometer tests

The UCS tests on 38 mm dia., 76 mm high, jacketed specimens and BT tests on 38–50 mm dia., 19 mm thick specimens gave the profiles included in Fig. 2. The UCS and BT tests advanced at 0.05 mm/min and reached failure within  $\approx 5$  to 10 min of loading. The shallower samples developed higher UCS strengths (up to 4.3 MPa) and greater

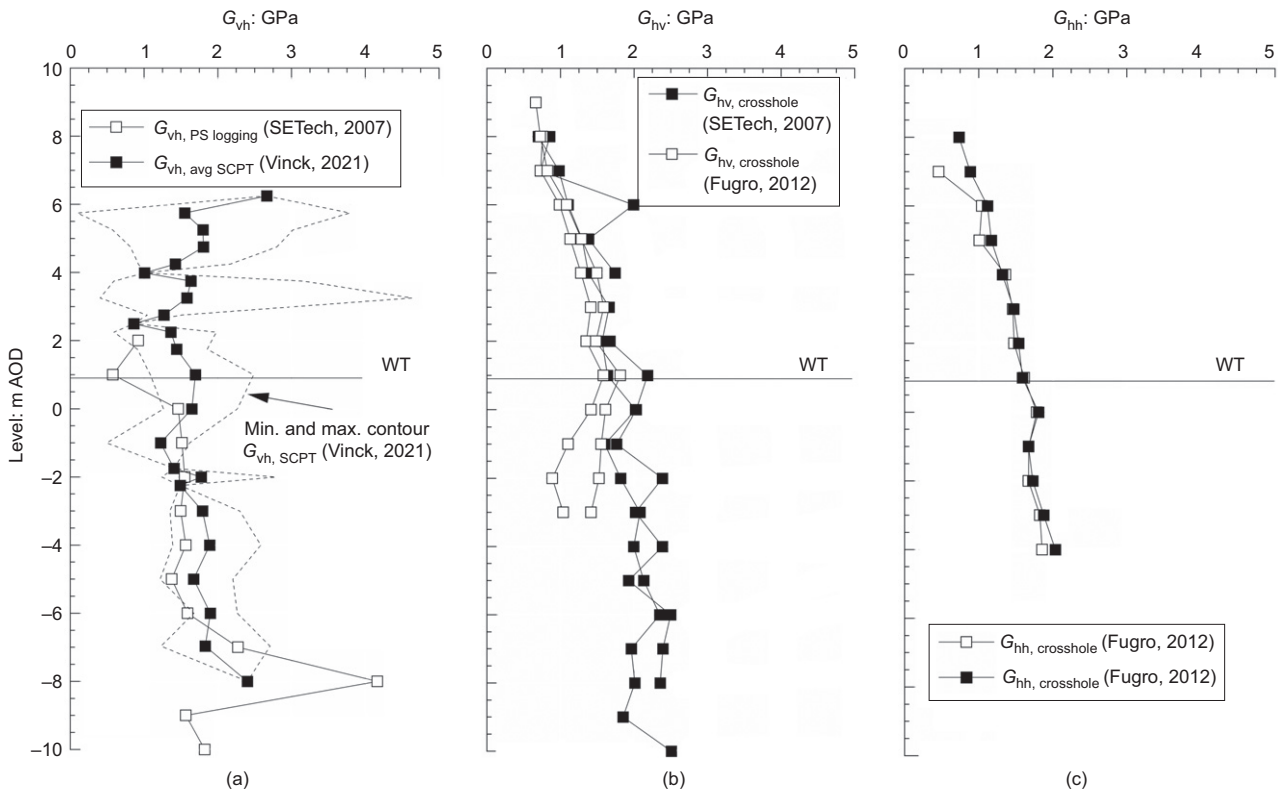


Fig. 4. Summary of shear stiffness profiles from (a) vertically travelling waves, and horizontally travelling waves with (b) vertical and (c) horizontal polarisation. From SCPT, PS logging and cross-hole testing at SNW

scatter, reflecting their partial saturation and suctions, the impact of which has been noted previously by De Gennaro *et al.* (2004) and Taibi *et al.* (2009) for chalk and Ciantia *et al.* (2015) for calcarenite. The tension BT strengths were  $\approx 1/10$ th of the UCS values.

Stage-loaded and constant-rate-of-strain (CRS) oedometer tests exhibited very stiff, quasi-elastic, initial one-dimensional (1D) behaviour, with minimal volumetric straining before yielding at the  $3.3 < \sigma'_{vy} < 6.9$  MPa points shown in Fig. 6, which are interpreted as reflecting in situ cementing and post-depositional geological disturbance, rather than the chalk's  $\approx 850$  m expected maximum burial depth (Mortimore, 2012).

The stage-loaded tests gave post-yield secondary compression (creep) indices  $C_{ac} = \Delta e / \Delta \log(t)$  of 0.016 to 0.018, indicating 0.043 to 0.048  $C_{ac}/C_c$  ratios that exceed Mesri & Vardhanabhuti's (2006) range for inorganic soils. Addis & Jones (1990) and Katsaros & Stone (2018) also note marked post-yield creep straining and strain rate dependency in chalk. The CRS tests, run at 0.6%/h, gave notably higher  $\sigma'_{vy}$  values than stage-loaded tests, which slowed to  $\approx 0.02\%/h$  after 24 h, suggesting strain rate dependency, as with natural clays (Nash *et al.*, 1992). An 'isotach' CRS test which switched between the standard rate and velocities ten times slower and then ten times faster, confirmed a 12% increase in vertical effective stress per ten-fold (post-yield) change in strain rate.

The SNW chalk's high average liquidity index (0.91) leads to its in situ  $e-\sigma'_v$  plotting well above the state limits that can be sustained by reconstituted specimens, as shown in Fig. 6 by the  $K_0$  normal compression line (NCL\*) of dried and ground chalk that was reconstituted by mixing to slurry at 1.4 times the liquid limit (LL). The intact post-yield compression curves trend towards the  $K_0$ -NCL\* at  $30 < \sigma'_v < 50$  MPa, as noted with calcarenites (Cuccovillo & Coop, 1999) but without converging, as expected for clays by Burland

(1990). The swelling curves confirm that the intact chalk's microstructure breaks down under high-pressure consolidation.

The SNW chalk's open vertical fissures indicate low  $K_0$ , despite its high prior burial depth.  $K_0$  cannot be measured reliably in chalk, so in situ stresses were assessed for testing assuming  $K_0 = 0.6$  (after Lord *et al.* (2002)) and accounting for measured field suctions, leading to  $30 < p'_0 < 160$  kPa over the testing depth range. Matching sets of specimens were tested after re-consolidation to both  $p'_0$  and  $p'_0 + 300$  kPa. The latter tests, which approached the cells' pressure limit for the deepest samples, indicated how the stress increases expected around the test piles might affect field behaviour.

*Triaxial and direct simple shear (DSS) programmes*

Five series of locally instrumented triaxial tests detailed in Table 2 investigated the stiffness and shear strength of the intact, saturated SNW chalk, providing additional information to the UCS tests on jacketed samples equipped with local axial strain sensors.

Series A. Undrained compression CIU (i.e. isotropically consolidated undrained triaxial compression) tests with pore pressure measurement on 38 mm dia., 76 mm high specimens consolidated isotropically to in situ  $p'_0$ .

Series B. As series A, but with drained compression CID (i.e. isotropically consolidated drained triaxial compression) testing to failure.

Series C. CID and CIU tests on 38 mm samples consolidated to in situ  $p'_0$  plus 300 kPa.

Series D. As series B, with 100 mm dia., 200 mm high specimens.

Series E. Non-destructive small-strain probing on 100 mm dia. specimens consolidated to a wide range of stress conditions, with dual-axis bender element testing.

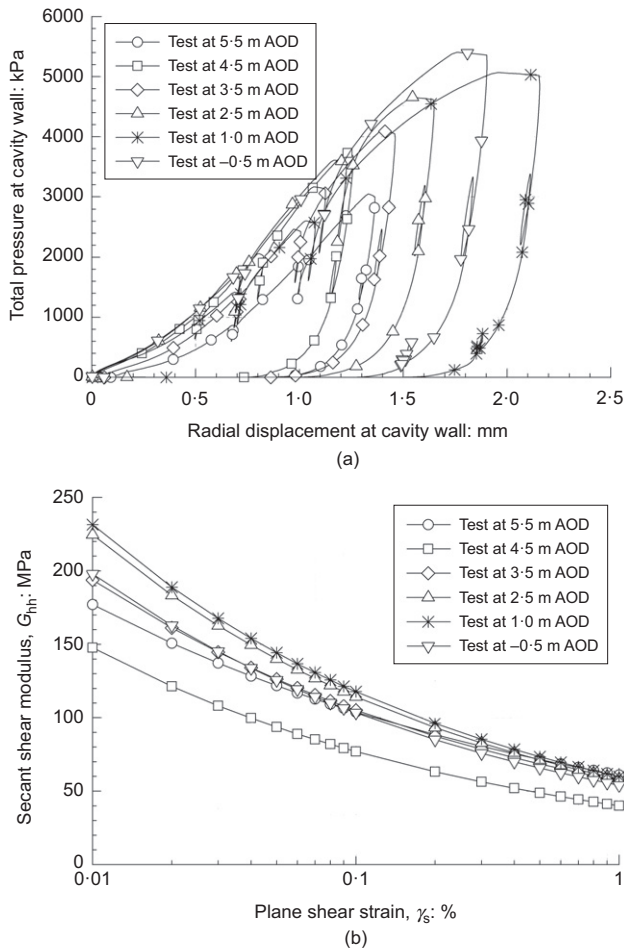


**Fig. 5. Pressure-meter tests: (a) overview of indicating loading/unloading cycles and creep stages and (b) secant shear moduli degradation plotted against plane shear strain, after Cambridge Insitu Ltd (2019)**

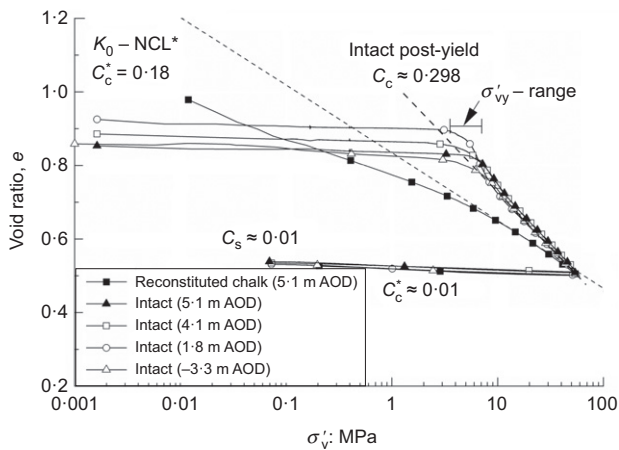


**Fig. 6. Compression response for reconstituted and intact chalk established from CRS ID compression tests**

Hydraulic stress-path cells rated to 4 MPa deviatoric stresses ( $q$ ) and 750 kPa cell and back-pressures were employed, with the local strain sensors that are essential to reliable stiffness determination (Jardine *et al.*, 1984; Tatsuoka *et al.*, 1999). ‘Floating’ pairs of linear variable differential transformers (LVDTs) and a ‘floating’ radial belt LVDT were deployed for 38 mm tests. The 100 mm dia. tests deployed three ‘floating’ vertical LVDTs and a three-point radial

**Table 2. Summary of triaxial test conditions and parameters for test series A–E**

Test series	Test code*	Depth: m BGL	Level: m AOD	$p'_0$ : kPa	$e_0^\dagger$	
A	IU-38-1	1.40	5.52	42	0.840	
	IU-38-2	2.40	4.52	52	0.803	
	IU-38-3	3.65	3.27	63	0.865	
	IU-38-4	6.34	0.59	88	0.805	
	IU-38-5	8.09	-1.17	100	0.879	
	IU-38-6	11.43	-4.51	123	0.836	
	IU-38-7	12.55	-5.63	131	0.829	
	IU-38-8	16.12	-9.20	156	0.842	
	B	ID-38-1	0.40	6.52	34	0.761
		ID-38-2	1.35	5.57	43	0.859
ID-38-3		2.40	4.52	52	0.824	
ID-38-4		3.65	3.27	63	0.766	
ID-38-5		5.59	1.33	85	0.794	
ID-38-6		7.51	-0.59	96	0.846	
ID-38-7		8.69	-1.77	104	0.825	
ID-38-8		10.77	-3.85	119	0.847	
ID-38-9		12.75	-5.83	133	0.805	
ID-38-10		16.12	-9.20	156	0.796	
C	ED-38-1	0.40	6.52	334	0.820	
	ED-38-2	1.35	5.57	343	0.843	
	ED-38-3	2.40	4.52	352	0.856	
	ED-38-4	3.65	3.27	363	0.846	
	ED-38-5	5.85	1.07	385	0.813	
	ED-38-6	7.51	-0.59	396	0.785	
	ED-38-7	8.69	-1.77	404	0.826	
	ED-38-8	11.05	-4.13	421	0.762	
	ED-38-9	12.75	-5.83	433	0.777	
	ED-38-10	16.12	-9.20	456	0.782	
	EU-38-11	1.40	5.52	342	0.808	
	EU-38-12	8.38	-1.46	402	0.802	
D	ID-100-1	0.40	6.52	34	0.879	
	ID-100-2	2.40	4.52	51	0.838	
	ID-100-3	3.65	3.27	64	0.818	
	ID-100-4	6.09	0.83	86	0.887	
	ID-100-5	7.36	-0.44	95	0.893	
	ID-100-6	8.55	-1.63	103	0.863	
	ID-100-7	11.22	-4.30	122	0.768	
	ID-100-8	12.75	-5.83	132	0.835	
	ID-100-9	15.84	-8.92	154	0.801	
E	P-100-1	0.40	6.52	34	0.840	
	P-100-2	2.40	4.52	51	0.825	
	P-100-3	5.85	1.07	84	0.817	
	P-100-4	12.60	-5.68	132	0.831	

\*Test code: I – in situ stresses ( $p'_0$ ); E – elevated pressure ( $p'_0 + 300$  kPa); P – probing test; U – undrained shearing in compression; D – drained shearing in compression; 38 – sample diameter (mm); 100 – sample diameter (mm).  
 $\dagger e_0$ : Void ratio prior to shearing.

sensing system; vertical and horizontal bender elements also enabled non-destructive  $G_{vh}$ ,  $G_{hv}$  and  $G_{hh}$  measurements. Liu (2018) summarises the equipment’s capabilities, sensitivities, resolutions and nominal precisions, noting that the 100 mm systems offer better resolution, finer stress control. Their larger sample volumes also accommodate the chalk’s structure more representatively. Neither system could apply the high cell pressures required to bring the chalk to failure in triaxial extension.

Specimens inevitably dried slightly during preparation, showing 70 to 80 kPa suctions on set-up that exceeded in situ  $p'$  at most levels; saturation was achieved by applying back-pressures (350 kPa or greater) until  $B > 0.95$ . Samples were swelled or compressed isotropically at 60 kPa/h to target  $p'_0$  values, which were maintained until volumetric creep rates reduced below 0.005% per day, requiring  $\approx 24$  and 48 h for the 38 mm and 100 mm specimens, respectively. The average

**Table 3. Summary of direct simple shear (DSS) test and specimen conditions (performed at Fugro GB Marine Limited)**

Test code	Depth: m BGL	Level: m AOD	$\sigma'_{v0}$ : kPa	$e_f$ *
DSS-1	0.40	6.52	46	0.645
DSS-2	2.40	4.52	71	0.702
DSS-3	5.00	1.92	104	0.810
DSS-4	8.10	-1.18	136	0.816
DSS-5	12.20	-5.28	175	0.837
DSS-6	14.85	-7.93	200	0.726

\* $e_f$ : Void ratio after shearing.

primary and secondary (creep) axial strains developed by consolidating isotropically to 300 kPa above  $p'_0$  in series C were 0.11% and 0.012%, respectively; the corresponding average radial strains were slightly greater at 0.13% and 0.031%. Creep straining is more pronounced under compression to higher pressures (ALPACA AWG, 2022). Monotonic shearing followed at 5% axial strain/day. System compliance and sample imperfections led to markedly lower local strain rates until peak deviator stresses were reached, on average, after 2.5 h of loading, although shearing continued for several days to capture post-peak trends.

Investigations were undertaken to establish the degree to which micro-fissures and other features might cause variations between tests on nominally identical samples. Repeat CIU tests on 38 mm dia. specimens cut from the same blocks indicated  $\pm 10\%$  lateral variations in  $s_u$  and greater variations in stiffness. Dispersion also arose due to minor vertical variations, with 100 mm dia. specimens showing less scatter than smaller samples. Drained tests gave more stable outcomes; check CID tests indicated only  $\pm 2\%$   $q_f$  variations between tests run at 0.5, 5, 50 and 500% per day, suggesting a minor influence of rate on strength, as with sands. However, non-linear stiffness was more markedly affected (Vinck, 2021).

Constant volume DSS tests were run (with Fugro GB Marine Ltd) at 5% shear strain/h employing 67 mm dia., 30 mm high samples and GDS Instruments ‘stacked-ring’ apparatus: see Table 3.

*Triaxial and UCS stress–strain behaviour*

Shearing behaviour is illustrated first by considering exemplar tests on saturated specimens sampled at -1.45 m ( $\pm 0.25$  m) AOD; later profiles summarise the key outcomes from all tests.

The stress–strain curves in Fig. 7 illustrate the general trend for UCS tests to manifest the most extended initial linear ranges and highest peak strengths among samples sheared from in situ  $p'_0$ . The slower triaxial tests showed non-linearity (or  $Y_1$  yielding (Jardine, 1992)) from smaller strains ( $\epsilon_a > 0.002\%$ ) and modest stiffness non-linearity, until brittle failure (or  $Y_3$  yielding) commenced at  $0.05\% < \epsilon_a < 0.2\%$  as the chalk lost bond strength and fractured. Intermediate  $Y_2$  yield points, identified in sands and clays by Kuwano & Jardine (2007), Gasparre *et al.* (2007) and others were not identified. The higher pressure CID test showed an anomalously soft concave upwards stress–strain curve over the intermediate strain range and required a larger than typical strain to reach failure. This feature is interpreted as reflecting randomly occurring relatively open micro-fissures (Kohata *et al.* (1997) or Tatsuoka *et al.* (1999)). Vinck (2021) encountered several similarly anomalous results in his 49 monotonic triaxial tests.

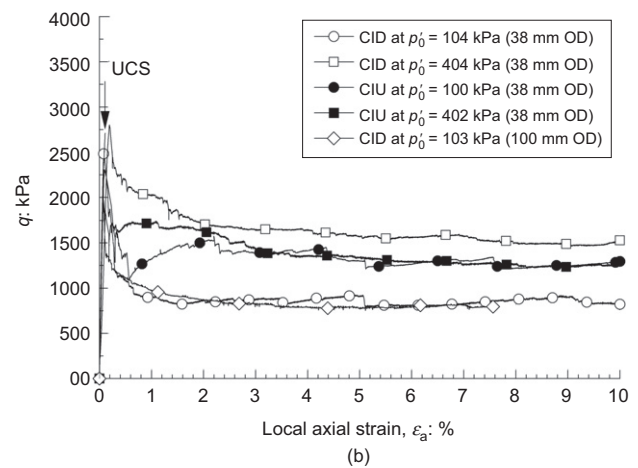
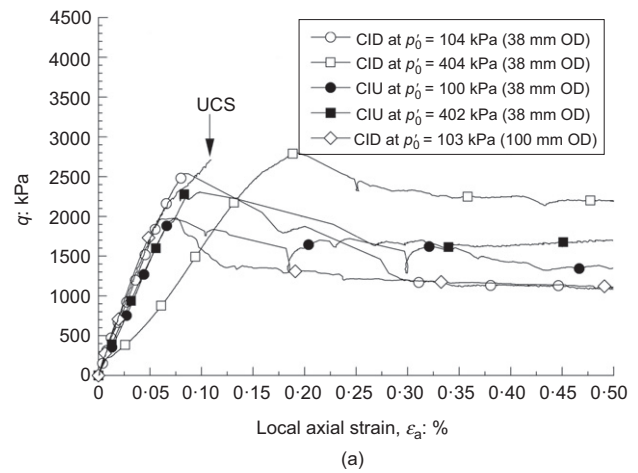


**Fig. 7. Deviatoric stress–axial strain trends for ‘deeper’ samples from -1.2 to -1.7 m AOD: (a) 0.5% axial strain range; (b) full strain range (OD, outer diameter)**

The 38 mm samples generally indicated drained pre-failure Poisson’s ratios ( $\nu'_{vh}$ ) between 0.2 and 0.3. However, the 100 mm dia. specimens’ three higher resolution radial sensors showed disparate trends around the specimens’ circumferences. This discontinuous response is interpreted as resulting from the low normal joint stiffnesses of partially open micro-fissures. More ‘continuous’ radial deformations and stiffer radial responses developed in most of the  $p'_0 + 300$  kPa experiments; higher pressure consolidation closes the micro-fissures more tightly and so increases normal stiffnesses.

*Triaxial effective stress paths*

The triaxial effective stress paths presented in Fig. 8 show peak  $q/p'$  ratios close to 3, the maximum that can be applied without the minor principal effective stress going into tension. Nevertheless, specimens sheared from in situ stresses developed vertical cracks and shear discontinuities as they failed, which often propagated upwards from the sample bases.

The CID triaxial tests showed marked ‘dilation’ as the specimens cracked and bifurcated. Such apparent ‘dilatancy’ is common in compression with rocks containing micro-fissures (Cerfontaine & Collin, 2018). Similar patterns were reflected in CIU tests, which showed strong pore pressure reductions as the samples failed and fractures tried to open.

The CIU tests’ pre-failure effective stress paths also approached the no-tension limit, following paths with initial gradients  $dp'/dq$  between 0.16 and 0.20, which

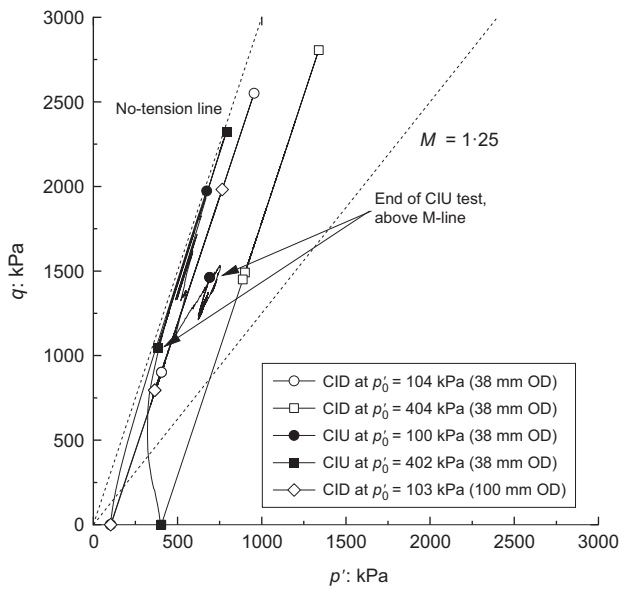


**Fig. 8.** Effective stress paths of drained and undrained triaxial tests from isotropic conditions for samples from  $-1.2$  m to  $-1.7$  m AOD

curved to the right as the tests progressed towards gradients close to the applied total stress  $dp/dq = 1/3$  ratio. The initial shear-induced pore pressure ratios  $A = du/dq$  (Skempton, 1954) fall around half the  $1/3$  ratio (equivalent to  $dp'/dq = 0$ ) expected for an isotropic elastic soil undergoing undrained compression. Cross-anisotropic elastic theory predicts  $A < 1/3$  when horizontal stiffness is less than vertical, with  $E'_h/E'_v < 1$  (Lings *et al.* (2000) or Kuwano & Jardine (2002)). Stiffness anisotropy is interpreted as the main reason for the low initial  $A$  values, as explored in later sections. The overall pore pressure changes tended to become closer to zero as the tests progressed and behaviour became progressively less elastic. CIU tests conducted after consolidation to  $p'_0 + 300$  kPa gave more vertical  $q-p'$  paths and  $A$  values compatible with  $E'_h \approx E'_v$ , before showing pore pressure changes close to zero at failure.

#### Triaxial effective stress peak shear strengths

The peak effective stress failure points from all triaxial tests are presented in Fig. 9. Interparticle bonding provides much of the specimens' peak resistance and the regressed  $q-p'$  peak failure line approximates a portion of the curved envelope implicit in critical state-based models of cemented calcareous media (Lagioia & Nova, 1995). Other criteria may be applied, including Hoek and Brown's expression. A regressed Mohr-Coulomb treatment gives  $c' = 0.49$  MPa,  $\phi'_{\text{peak}} = 39.6^\circ$ . ALPACA AWG (2022) show how consolidation to higher pressures damages the bonding, promotes a more ductile and 'frictional' shearing response with a curved yield envelope with  $M = 1.25$  or  $\phi'_{\text{cs}} \approx 31^\circ$  at critical state and implies pressure-dependent  $c'$  and  $\phi'_{\text{peak}}$  for dry of critical conditions. The  $v-p'$  states given by equation (1) held at critical states, where  $v = 1 + e$  and  $p'_{\text{ref}}$  corresponds to 1 kPa in the units adopted

$$v = 2.155 - 0.08 \times \ln p / p'_{\text{ref}} \quad (1)$$

The non-uniform bifurcation mechanisms that apply post-peak cannot be interpreted as single-element tests represented by 'continuum-mechanics'  $q/p'$  measures. However, Coulomb analyses of failure planes can identify 'post-rupture' strengths (Burland, 1990). Resolving shear and normal forces acting on planes measured at  $60-65^\circ$  to the

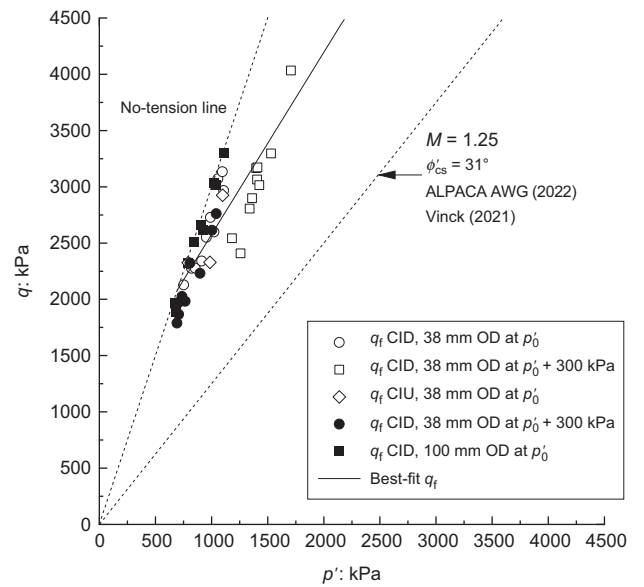


**Fig. 9.** Peak shear strengths and failure criteria for intact chalk

horizontal after testing indicates post-rupture  $\phi' = 35^\circ \pm 5^\circ$  if  $c' = 0$ , although other combinations with lower  $\phi'$  and higher  $c'$  can be drawn through the scattered post-rupture trends.

#### Constant volume DSS tests

Simple shear (DSS) testing is difficult with chalk, as local slippage or putty formation may occur near the platens. Alternative fixing arrangements were trialled before the six successful reported tests were completed. The DSS boundary conditions limit the scope for large displacements to develop on bifurcations. They also impose large principal stress axis rotations, which can lead to lower strengths in anisotropic soils. Hollow cylinder apparatus (HCA) tests show that the minor principal stresses may tend towards tensile values in simple shear tests conducted on bonded geomaterials from relatively initial mean stresses (Brosse *et al.*, 2017).

Figure 10 presents the  $(\tau, \sigma'_v)$  DSS 'effective stress path' followed by a chalk sample from a similar ( $-1.2$  m AOD) level to the exemplar triaxial tests. The points at which shear strains (from 0.1 to 20%) were attained are indicated, as are failure points from the five other tests. All showed clockwise stress-path rotations (indicating  $Y_3$  yielding) after relatively short, near-vertical, initial sections. Relatively soft non-linear 'dilative' paths followed until failure after large strains, with  $5\% < \gamma_f < 12\%$ . However, the peak  $s_u$  values (taken as peak  $\tau_{vh}$ ) were, on average  $\approx 45\%$  lower than in the CIU tests. Applying conventional Coulomb analysis, the average ultimate  $\tau/\sigma'_v \approx 0.61$  ratio indicates  $\phi' \approx 31^\circ$  if  $c' = 0$  kPa, comparable to the pressure meter and triaxial critical-state strengths. Tension cracks were evident on dismantling that contributed to the low resistances.

#### Stiffness

Figure 11 presents the exemplar triaxial and (locally instrumented) UCS tests' drained (CID)  $E'_v$  and undrained (CIU and UCS)  $E'_v$  vertical stiffness-strain trends. Linear regressions established pre- $Y_1$  (drained or undrained) linear initial moduli followed by non-linear secant variations up to peak  $q$ . As noted earlier, the CID test's lower stiffness was untypical and is interpreted as being attributable to its micro-fissures being unusually open and compliant. The larger 100 mm specimens show the most systematic decays



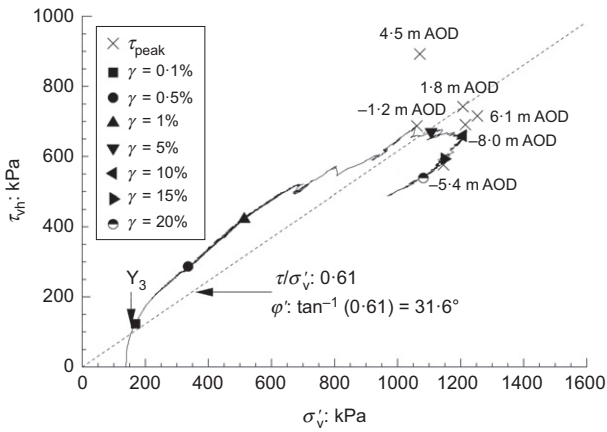


Fig. 10. Effective stress paths of constant-volume DSS tests on sample from -1.2 m AOD ( $\sigma'_v = 136$  kPa) and ultimate points from five other depths

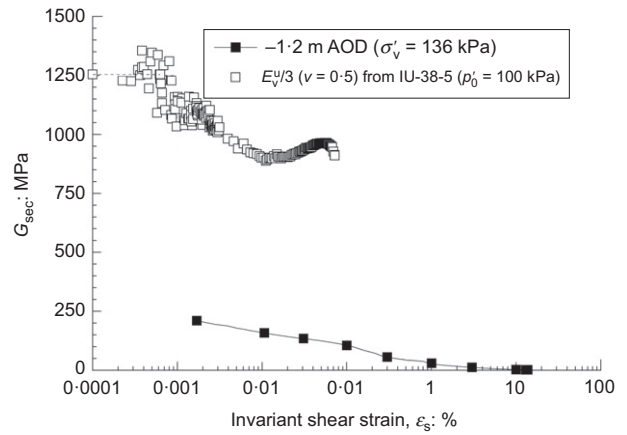


Fig. 12. Shear stiffness moduli degradation of constant-volume DSS and CIU tests for samples from -1.2 m AOD

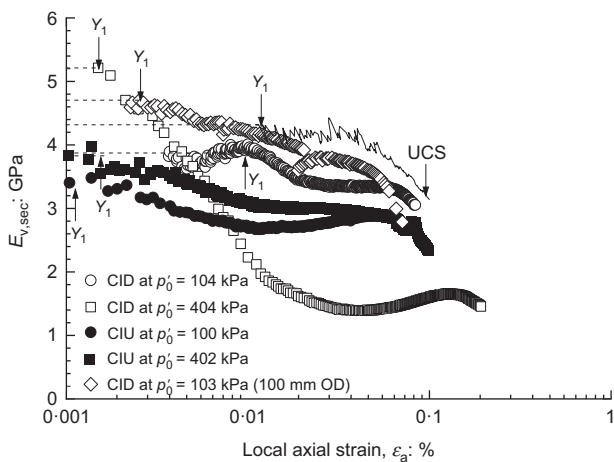


Fig. 11. Secant Young's moduli degradation of drained and undrained triaxial tests from isotropic conditions for samples from -1.2 m to -1.7 m AOD

in stiffness after undergoing  $Y_1$  yielding, while the smaller samples' CID and CIU curves showed more variable behaviour. Even large increases in consolidation pressures have only a modest effect on vertical stiffness (ALPACA AWG, 2022).

It is interesting that the CIU  $E'_v$  traces fall well below the CID  $E'_v$  curves. With isotropic elastic media  $E'_h/E'_v = 3/(2(1 + \nu'))$  and so exceeds unity if  $\nu'$  is less than 0.5. However,  $E'_v$  can exceed  $E'_h$  in cross-anisotropic soils if, as argued earlier,  $E'_h < E'_v$  and plausible cross-anisotropic Poisson's ratios apply.

The typical DSS test from -1.2 m AOD shown in Fig. 12 indicated equivalent secant shear stiffness  $G_{sec}$  falling steeply with invariant shear strain  $\epsilon_s (= \gamma/\sqrt{3})$  from an initial maximum of 210 MPa at  $\approx 0.002\%$ . The DSS tests were unable to resolve any initial linear range and the triaxial CIU tests' octahedral shear stiffnesses, calculated as  $G_{tr1} = E'_v/3$  with  $\epsilon_s = \epsilon_a$ , far exceed the reported DSS maximum moduli at all depths considered. The discrepancy may reflect non-uniform strains developing near platens, as well as the DSS tests' early yielding identified in Fig. 10.

PROFILES OF STRENGTH AND STIFFNESS

Profile plots summarise how mechanical properties vary with depth, test stress path and pressure level.

Total stress peak shear strengths

The peak deviator stress  $q_f$  and  $s_u$  trends are presented in Fig. 13, showing that the (jacketed) UCS tests  $q_f$  values exceed those of the fully saturated triaxial tests by, on average,  $\approx 22\%$ . The higher UCS strengths reflect their specimens' generally higher effective stresses (with suctions of 70 to 80 kPa on set-up that generally exceeded the triaxial tests' imposed in situ  $p'_0$  values), incomplete saturation (especially above the water table) and potentially their  $\approx 24$  times faster strain rates to failure. The UCS strengths also appear  $\approx 45\%$  higher than expected from Matthews & Clayton's (1993) correlation with IDD, emphasising the value of site-specific testing.

Considering next the effects of drainage, the saturated 38 mm peak triaxial  $q_f$  trends covering in situ  $p'_0$  conditions, the undrained CIU tests (with  $s_u = q_f/2$ ) give only slightly higher  $q_f$  values than drained CID tests in the (shallow) Margate Chalk, and vice versa in the deeper Seaford. As noted earlier, little overall undrained pore pressure generation occurred prior to failure.

The checks on CID sample size effects indicated generally lower  $q_f$  and less scattered values for 100 mm than 38 mm dia. specimens, as is often the case for soils possessing pronounced meso-structure, although the trends converged better at depth, reflecting fissures becoming tighter and more widely spaced.

A further feature examined in Fig. 13 is the impact of the 300 kPa consolidation pressure increases applied in series B and C. The 'elevated'  $q_f$ -depth trend plots  $\approx 25\%$  above the 'in situ' series at shallow depth and  $\approx 15\%$  above it at greater depth, reflecting the reducing intensity of discontinuities with depth. Consolidation to higher stresses causes gains in 'frictional' strength along with damage to bonding (ALPACA AWG, 2022). Finally, the DSS  $s_u$  trends (taken as peak  $\tau_{vh}$ ) data plot consistently (by  $\approx 45\%$ ) below the CIU triaxial test outcomes.

CPTu penetration tests are often employed to gauge in situ  $s_u$  values for fine-grained soils through empirical  $N_{kt}$  cone factors, assuming correlation of  $q_t = N_{kt} \times s_u + \sigma_{v0}$ . The profiles shown in Figs 2 and 13 indicate  $N_{kt}$  values of  $12 \pm 3$  and  $21 \pm 4$  with respect to CIU and DSS  $s_u$ , respectively.

Stiffness

Equivalent profiles of initial vertical Young's moduli plotted in Fig. 14 identify how drainage condition, sample size, elevated pressures and shearing conditions affect

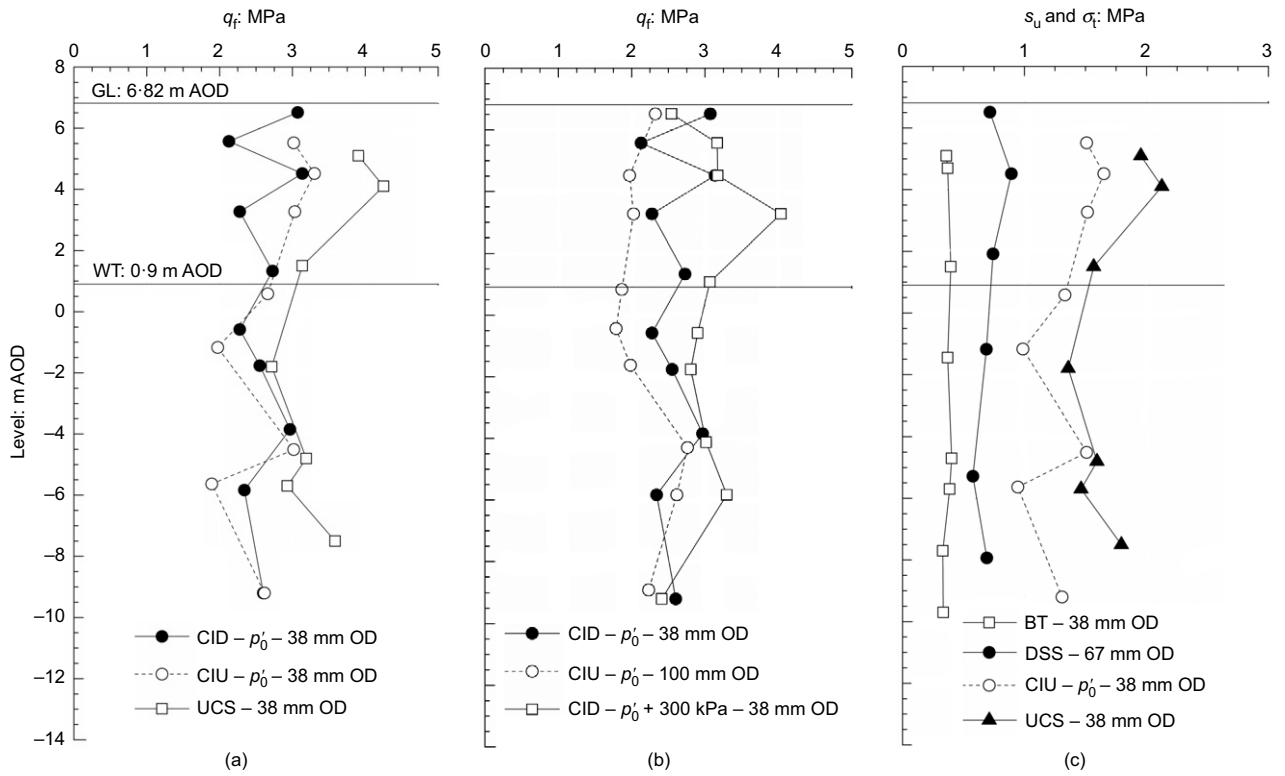


Fig. 13. Profiles of peak compressive strength,  $q_f$ , considering the effect of: (a) drainage condition; (b) sample size and elevated pressure; and (c) loading condition

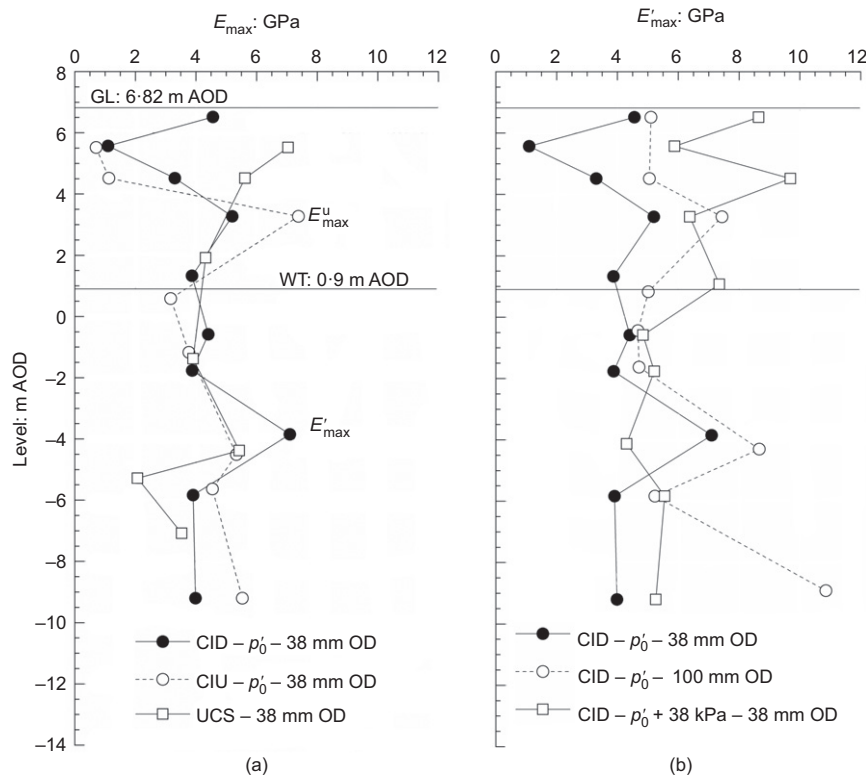
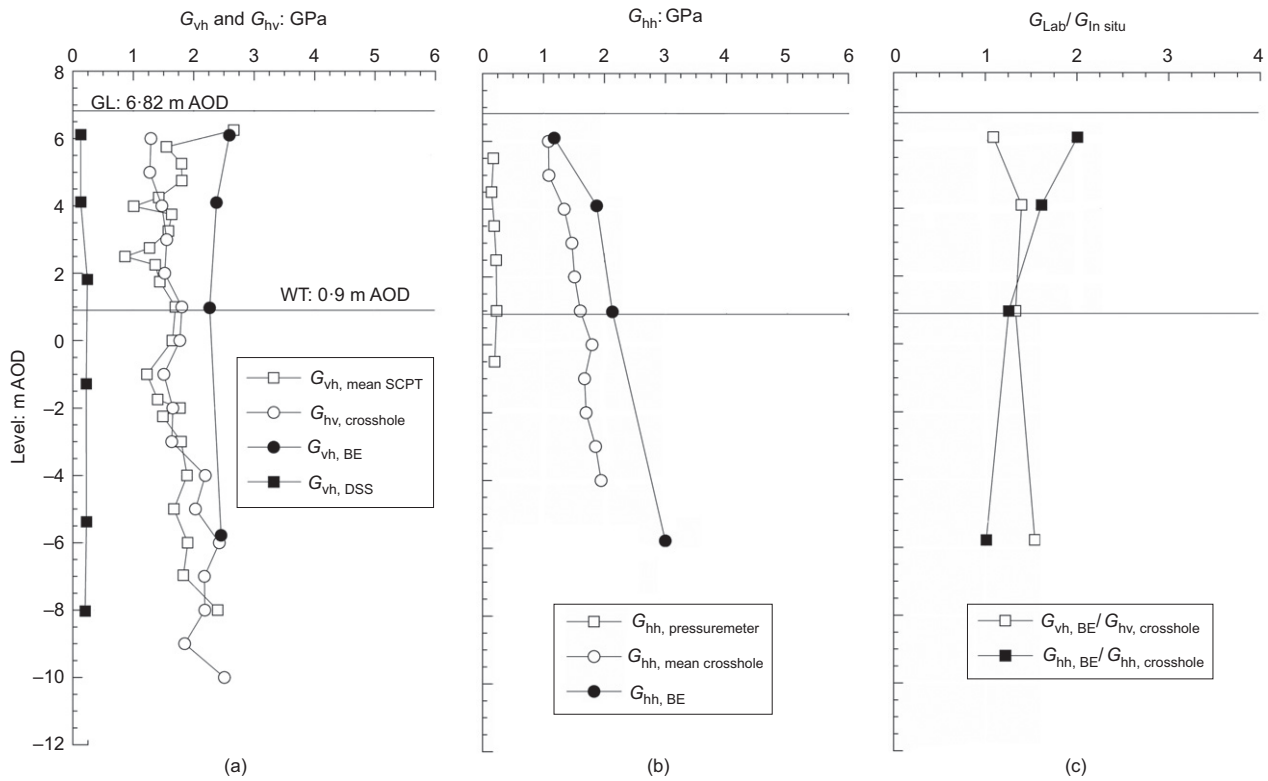


Fig. 14. Profiles of secant Young's moduli,  $E_{max}$ , considering the effect of: (a) drainage and loading condition; (b) sample size and elevated pressure

stiffness. The locally instrumented triaxial and UCS moduli are broadly comparable, although the latter show more scatter and longer linear ranges. The unusual hierarchy between drained and undrained moduli is confirmed, with  $E'_{v,max}$  exceeding  $E^u_{v,max}$  in most cases. Elevating the initial

mean effective stress by 300 kPa raised  $E'_{v,max}$  by  $\approx 55\%$  over the first 6 m, but had less impact at greater depth. This gain, which exceeds that noted for shear strength, is interpreted reflecting the closure of micro- and meso-fissures, which are more prominent and have wider apertures at shallow depth. It



**Fig. 15.** (a) Profiles and ratios of shear stiffness  $G_{vh}$  measured in the laboratory and in situ; (b)  $G_{hh}$  measured in the laboratory and in situ; and (c) with field measurements

is also clear that the 100 mm dia. triaxial samples'  $E'_{v,max}$  exceed those from the smaller specimens, by an average of  $\approx 45\%$  (excluding one outlier), which may reflect the larger equipment's better stress/strain uniformity and higher resolution measurements.

Figure 15 considers the shear stiffnesses defined at the smallest strains offered by various field and laboratory techniques. Such profiles may vary due to specimen disturbance, anisotropy, meso-structure and differing strain rates, as well as variable stress and strain levels, test volumes and instrument resolutions. Comparing laboratory Bender Element shear wave velocities with identically oriented in situ values allows the combined effects of sampling disturbance and meso-fabric to be assessed. While profiles vary across the site, the mean seismic CPT  $G_{vh}$  and cross-hole  $G_{hv}$  trends fall well below the near-ground-surface triaxial Bender Element (BE)  $G_{vh}$  measurements, before converging with increasing depth. This trend is interpreted as reflecting the impact of any open fissures, which are systematically avoided when preparing laboratory specimens, occurring less frequently at depth. The DSS  $G_{vh}$  maxima fall far below those interpreted from either laboratory or field shear wave velocities, confirming the tests' inability to resolve elastic moduli.

Figure 15 also contrasts the cross-hole, BE  $G_{hh}$  and pressure-meter  $G_{hh}$  (measured at 0.01% shear strain) trends. The BE tests show higher stiffnesses than the seismic field measurements, with laboratory-to-field ratios of 1.1 to 1.5, confirming the systematic impact of meso-structure. As with the DSS tests, the pressure-meter data fall far below the geophysical measurements and reflect the larger-strain behaviour of more disturbed material.

#### Stiffness anisotropy

The CIU tests' effective stress path inclinations and the systematic trend for initial  $E'_v$  to exceed  $E'_v^u$  indicated that the

chalk's vertical moduli exceed equivalent horizontal stiffnesses under in situ stress conditions. Series E explored anisotropy more precisely through high-resolution BE and monotonic stress probing experiments. Fig. 16 presents first the field and laboratory tests'  $G_{hh}/G_{vh}$  profiles. The triaxial BE measurements (made on the same samples) gave  $G_{hh}/G_{vh} \approx 0.5$  in the shallow layers and tended to ratios exceeding unity at depth. The equivalent field seismic data show a similar, but more muted, trend.

The series E tests applied small-strain axial and radial drained probes to assess any elastic, fully recoverable behaviour with the chalk's  $Y_1$  kinematic yield surfaces. The vertical stiffnesses are found easily from the high-resolution axial stress and strain measurements. Assessment of horizontal stiffnesses is less direct. Kuwano & Jardine (2002) give alternative routes for deriving full sets of cross-anisotropic compliance parameters from combined radial probing tests, which define the parameter  $R$  in equation (2) below and BE  $G_{hh}$  measurements. However, even small radial increments applied from in situ stresses led to responses that were hysteretic and non-uniform around the samples' perimeters, reflecting the presence of imperfectly closed, mainly vertical, micro-fissures. Treating the chalk as an elastic continuum led to implausible cross-anisotropic  $\nu'_{hv}$  ratios in some cases, because the samples' radial behaviour was neither continuous nor fully recoverable, even at very small strains. Vinck (2021) shows that equation (3) provides robust assessments of horizontal stiffness  $E'_{h,max}$  as it contains no Poisson ratio terms.

$$R = \Delta\sigma'_h / \Delta\epsilon_h \text{ (under axisymmetric triaxial conditions)} \quad (2)$$

$$E'_h = \frac{4RG_{hh}}{R + 2G_{hh}} \quad (3)$$

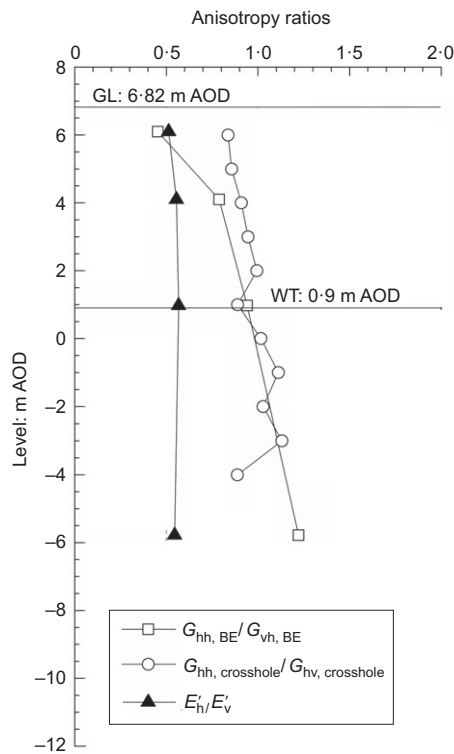


**Fig. 16. Profiles of stiffness anisotropy as obtained from bender measurements and cross-hole investigations and suites of drained and undrained triaxial probing tests**

The  $E'_h/E'_v$  profile developed from four suites of probing tests in Fig. 15 confirms that horizontal loading from in situ stresses provokes a far softer response than vertical compression, which is important when analysing lateral pile loading. Vinck (2021) shows that anisotropy diminishes after consolidation to higher pressures.

#### KEY FEATURES FOR PRACTICAL ANALYSES

The characterisation research identifies aspects of behaviour that require attention when attempting to model practical problems in chalk. Pedone *et al.* (2020) describe how these aspects were addressed in advanced 3D finite-element modelling of the ALPACA lateral pile load tests, showing how the SNW characterisation research was applied to capture full-scale field behaviour.

The selection of parameters and constitutive models for reliable and representative predictions of field shear strengths depends on the boundary conditions, pressures and scales of the problem considered. The most important aspects to recognise at 'routine' mean stresses are: (a) chalk's propensity to tensile fracture when sheared; (b) the fragile nature of its compressive shear strength; and (c) its rapid degradation from peak to post-rupture strengths. It is equally vital to recognise that ductile behaviour and stable critical state resistances apply after consolidation to  $p'_0 > 2$  MPa (ALPACA AWG, 2022). Strain softening and destructuration in both laboratory DSS and full-displacement field pressure-meter tests indicate 'operational' shear strengths far below the triaxial or UCS peak values. Interfaces between chalk masses and structural elements also require careful consideration. Vinck (2021) reports that putty formed around pile shafts develops angles  $\delta'$  of 31° to 34° when sheared against a range of rough steel interfaces, when tested with a spread of pore-fluid sodium chloride concentrations and at a broad range of ages.

Analysts must also consider stiffness. The monotonic triaxial, laboratory BE and field geophysical measurements indicate remarkably high elastic moduli. Modelling must also capture the chalk's non-linear pre-failure behaviour; locally instrumented triaxial tests show how vertical moduli vary with strain level and provide the basis for fitting suitable non-linear pre-failure models. Stiffness is markedly anisotropic under in situ conditions with the response to horizontal loading being around half as stiff as expected from laboratory compression tests. While meso-structural factors lead to field velocities being lower than laboratory equivalents, body waves can follow branched pathways that circumvent discontinuities and micro- to macro-fissures may have a still greater impact on mass stiffness under field loading (Matthews & Clayton, 1993).

The characterisation study also confirmed that chalk is susceptible to creep straining and shows strain-rate-dependent compressibility, both under in situ pressures (due to micro-fissure closure) and at higher stresses, when bond breakage and pore space collapse occur.

#### SUMMARY AND CONCLUSIONS

The characterisation study applied advanced testing to establish how the properties of low- to medium-density chalks vary with applied stress conditions, depth and structure. Although the programme was designed to support and enable modelling of the ALPACA pile tests, the outcomes are relevant to a wide range of other geotechnical problems in chalk and comparable geomaterials. The key conclusions are given below.

- Intact chalk exists at states it cannot sustain when reconstituted. It is highly sensitive and destructures when taken to large strains, especially under high-impact dynamic loading, leading to remarkably high CPTu pore pressures and putty formation around pile shafts during installation.
- Destructuration and tensile failure affect the responses seen in field and laboratory shear tests; they also affect full-scale pile behaviour.
- A clear hierarchy exists between strengths obtained from UCS, BT, saturated triaxial and DSS tests conducted from in situ stress conditions. The relatively high UCS strengths reflect partial specimen saturation and potentially rate effects, while the DSS and BT tests' low resistances reflect the chalk's fragile response to tension loading.
- Slow drained (CID) and undrained (CIU) triaxial compression tests develop markedly brittle failures after relatively small axial strains (around 0.15%). The closely similar CID and CIU effective stress path inclinations developed under in situ stresses reflect marked stiffness anisotropy, with  $E'_h < E'_v$ .
- Specimen scale affects CID test outcomes. 100 mm dia. specimens are generally slightly weaker than 38 mm dia. samples, but are noticeably stiffer due to the influence of both micro-fissures and test conditions. Where practically feasible, well-instrumented tests on large specimens should be preferred.
- Under routine pressures the chalk's effective stress peak compressive shear strengths includes a substantial proportion of bonded strength. However, this decays rapidly post-peak to give low post-rupture strengths. Fully destructured chalk develops well-defined critical state shearing resistance and void ratio–pressure relationships. Cone–pressure-meter tests appear to reflect the properties of destructured chalk.

- (g) Profiles of  $G_{hh}$  and  $G_{vh}$  from in situ and laboratory dynamic testing show similar depth trends. While laboratory tests over-record bulk stiffness systematically by avoiding all large fissures, field geophysical tests reveal similar patterns for  $G_{hh}/G_{vh} < 1$  at shallow depth and  $E'_h/E'_v < 1$  throughout that are interpreted as resulting from micro-fissures. Samples consolidated to pressures that close these fissures show far less anisotropy, while full displacement pressure-meter tests indicate substantially lower shear stiffness.
- (h) Laboratory and field tests in chalk indicate high levels of creep straining as well as strain-rate-dependent compressibility and stiffness; further investigation is warranted on these aspects.

ACKNOWLEDGEMENTS

The ALPACA and ALPACA Plus projects were funded by the Engineering and Physical Science Research Council's (EPSRC) grant EP/P033091/1, Royal Society Newton Advanced Fellowship NA160438 and Supergen ORE Hub 2018 (EPSRC EP/S000747/1). Byrne is supported by the Royal Academy of Engineering under the Research Chairs and Senior Research Fellowships scheme, while Imperial College's EPSRC Centre for Doctoral Training (CDT) in Sustainable Civil Engineering and the DEME Group (Belgium) supported Ken Vinck's doctoral study (EPSRC EP/L016826/1). The authors would like to express their gratitude to the joint industry project industrial partners: Atkins, Cathie Associates, Equinor, Fugro, Geotechnical Consulting Group (GCG), Iberdrola, Innogy, LEMS, Ørsted, Parkwind, Siemens-Gamesa, Scottish Power Renewables, Vattenfall and TATA steel for their substantial financial and technical support. Imperial College technicians Steve Ackerley, Graham Keefe, Prash Hirani, Stef Karapanagiotidis, Graham Nash and Gary Jones are thanked for their invaluable expert work. The authors also acknowledge contributions to CPT and pressure-meter testing, block sampling, rotary core sampling, piezometer installation and monitoring and DSS testing by Cambridge Insitu Ltd, Fugro Ltd, Geotechnical Observations Ltd, Lankelma Ltd and Socotec UK Ltd.

NOTATION

$A$	pore-pressure coefficient
$B$	pore-pressure coefficient
$C_c, C_c^*$	compressibility index for intact and reconstituted specimen
$C_s, C_s^*$	swelling index for intact and reconstituted specimen
$C_{ae}$	secondary compression index
$c'$	soil cohesion
$c_{h,piezo}$	radial coefficient of consolidation
$E$	specimen void ratio
$E'_h, E'_v$	drained Young's moduli for cross-anisotropic elastic soil
$E''_h, E''_v$	undrained Young's moduli for cross-anisotropic elastic soil
$G_{hh}$	shear modulus in the horizontal plane
$G_{vh}, G_{vh}$	shear modulus in the vertical plane
$G_s$	specific gravity
$K_o$	earth pressure coefficient at rest
$k_v$	vertical permeability
$M$	critical state stress ratio, $(q/p')_{cs}$
$N_{kt}$	empirical cone factor
$n$	porosity
$p'$	mean effective stress
$p'_0$	initial mean effective stress
$Q$	deviatoric stress $(= \sigma'_a - \sigma'_r)$
$q_f$	deviatoric stress at failure
$q_t$	corrected cone tip resistance

$q_u$	unconfined compressive strength
$R$	radial effective stiffness
$S_r$	saturation degree
$s_u$	undrained shear strength
$t$	time
$t_{50}$	time for 50% dissipation of excess pore water pressure
$u_1$	pore pressure measured at the cone tip
$u_2$	pore pressure measured at the cone shoulder
$V$	specific volume
$w$	water content
$Y_1, Y_2, Y_3$	soil yielding surfaces defined in the multiple yielding surface framework, details by Jardine (1992)
$\gamma_s$	plane shear strain
$\epsilon_a$	axial (vertical) strain
$\epsilon_h$	radial (horizontal) strain
$\rho_b$	bulk density
$\rho_d$	dry density
$\sigma'_r$	radial effective stress
$\sigma'_t$	indirect tensile strength
$\sigma'_v, \sigma'_a$	vertical (axial) effective stress
$\sigma'_{vy}$	effective vertical yield stress
$\nu'$	Poisson's ratio
$\phi', \phi'_{peak}, \phi'_{cs}$	shear resistance angle at peak and critical state
$\Psi$	dilation angle

REFERENCES

Addis, M. & Jones, M. (1990). Mechanical behaviour and strain rate dependence of high porosity chalk. In *Chalk: proceedings of the international chalk symposium held at Brighton Polytechnic on 4-7 September 1989*, pp. 239–244. London, UK: Thomas Telford.

Ahmadi-Naghadeh, R., Liu, T., Vinck, K., Jardine, R. J., Kontoe, S., Byrne, B. W. & McAdam, R. A. (2022). Laboratory characterization of the response of intact chalk to cyclic loading. *Geotechnique*, <https://doi.org/10.1680/jgeot.21.00198>.

ALPACA AWG (Academic Work Group) (2022). Appendix chapter 2: joint UCL high pressure study. In *Final interpretive report*. London, UK: Imperial College London and University of Oxford.

Alvarez-Borges, F. J. A. (2019). *The shaft capacity of small displacement piles in chalk*. PhD thesis, University of Southampton, Southampton, UK.

ASTM (2019). D4543-19: Standard practices for preparing rock core as cylindrical test specimens and verifying conformance to dimensional and shape tolerances. ASTM International, West Conshohocken, PA, USA, <https://doi.org/10.1520/D4543-19>.

Barbosa, P., Geduhn, M., Jardine, R. J., Schroeder, F. C. & Horn, M. (2015). Offshore pile load tests in chalk. In *Geotechnical engineering for infrastructure and development: XVI European conference on soil mechanics and geotechnical engineering* (eds M. G. Winter, D. M. Smith, P. J. L. Eldred and D. G. Toll), vol. 6, pp. 2885–2890. London, UK: ICE Publishing.

Barbosa, P. M., Geduhn, M., Jardine, R. J. & Schroeder, F. C. (2017). Large scale offshore static pile tests – practicality and benefits. In *Offshore site investigation and geotechnics – smarter solutions for offshore developments*, vol. 2, pp. 644–651. London, UK: Society for Underwater Technology.

Bialowas, G. A. (2017). *Time and stress dependent mechanical properties of reconstituted chalk*. PhD thesis, University of Bristol, Bristol, UK.

Bolton, M. D. & Whittle, R. W. (1999). A non-linear elastic/perfectly plastic analysis for plane strain undrained expansion tests. *Geotechnique* **49**, No. 1, 269–292, <https://doi.org/10.1680/geot.1999.49.1.133>.

Brosse, A. M., Jardine, R. J. & Nishimura, S. (2017). The undrained shear strength anisotropy of four Jurassic to Eocene stiff clays. *Geotechnique* **67**, No. 8, 653–671, <https://doi.org/10.1680/jgeot.15.P227>.

Buckley, R. M. (2018). *The axial behaviour of displacement piles in chalk*. PhD thesis, Imperial College London, London, UK.

Buckley, R. M., Jardine, R. J., Kontoe, S., Parker, D. & Schroeder, F. C. (2018). Ageing and cyclic behaviour of axially loaded piles driven in chalk. *Geotechnique* **68**, No. 2, 146–161, <https://doi.org/10.1680/jgeot.17.P012>.

- Buckley, R. M., Jardine, R. J., Kontoe, S., Barbosa, P. & Schroeder, F. C. (2020a). Full-scale observations of dynamic and static axial responses of offshore piles driven in chalk and tills. *Geotechnique* **70**, No. 8, 657–681, <https://doi.org/10.1680/jgeot.19.T1.001>.
- Buckley, R. M., Jardine, R. J., Byrne, B. W., Kontoe, S., McAdam, R. A., Ahmadi-Naghadeh, R., Liu, T. F., Schranz, F. & Vinck, K. (2020b). Pile behaviour in low–medium density chalk: preliminary results from the ALPACA project. In *Proceedings of the fourth international symposium on frontiers in offshore geotechnics (ISFOG)* (ed. Z. Westgate). Hawthorne, NJ, USA: Deep Foundation Institute.
- Bundy, S. P. S. (2013). *Geotechnical properties of chalk putties*. PhD thesis, University of Portsmouth, Portsmouth, UK.
- Burland, J. B. (1990). On the compressibility and shear strength of natural clays. *Geotechnique* **40**, No. 3, 329–378, <https://doi.org/10.1680/geot.1990.40.3.329>.
- Carotenuto, P., Meyer, V., Strøm, P. J., Cabarkapa, Z., St. John, H. & Jardine, R. J. (2018). Installation and axial capacity of the Sheringham Shoal offshore wind farm monopiles – a case history. In *Engineering in chalk: proceedings of the chalk 2018 conference* (eds J. A. Lawrence, M. Preene, U. L. Lawrence and R. M. Buckley), pp. 117–122s. London, UK: ICE Publishing.
- Carrington, T. M., Li, G. & Rattley, M. J. (2011). A new assessment of ultimate unit friction for driven piles in low to medium density chalk. In *Proceedings of the 15th European conference on soil mechanics and geotechnical engineering: geotechnics of hard soils – weak rocks (part 4)* (eds A. Anagnostopoulos, M. Pachakis and C. Tsatsanifos), pp. 825–830. Amsterdam, the Netherlands: IOS Press.
- Cerfontaine, B. & Collin, F. (2018). Cyclic and fatigue behaviour of rock materials: review, interpretation and research perspectives. *Rock Mech. Rock Engng* **51**, No. 2, 391–414.
- Ciantia, M. O., Castellanza, R. & Di Prisco, C. (2015). Experimental study on the water-induced weakening of calcarenites. *Rock Mech. Rock Engng* **48**, No. 2, 441–461.
- Ciavaglia, F., Carey, J. & Diambra, A. (2017a). Time-dependent uplift capacity of driven piles in low to medium density chalk. *Geotechnique Lett.* **7**, No. 1, 90–96, <https://doi.org/10.1680/jgele.16.00162>.
- Ciavaglia, F., Carey, J. & Diambra, A. (2017b). Monotonic and cyclic lateral tests on driven piles in Chalk. *Proc. Instn Civ. Engrs – Geotech. Engng* **170**, No. 4, 353–366, <https://doi.org/10.1680/jgeen.16.00113>.
- Clayton, C. R. I. (1977). Some properties of remoulded chalk. In *Proceedings of the 9th international conference on soil mechanics and foundation engineering*, pp. 65–68. Tokyo, Japan: Japanese Society of Soil Mechanics and Foundation Engineering.
- Clayton, C. R. I., Gordon, M. A. & Matthews, M. C. (1994). Measurements of stiffness of soils and weak rocks using small strain laboratory tests and field geophysics. In *Pre-failure deformation of geomaterials* (eds S. Shibuya, T. Mitachi and S. Miura), pp. 229–234. Rotterdam, the Netherlands: Balkema.
- Clayton, C. R. I., Matthews, M. C. & Heymann, G. (2002). The chalk. In *Characterisation and engineering properties of natural soils* (eds T. S. Tan, K. K. Phoon, D. W. Hight and S. Leroueil), vol. 2, pp. 1402–1434. Rotterdam, the Netherlands: Balkema.
- Collin, F., Cui, Y. J., Schroeder, C. & Charlier, R. (2002). Mechanical behaviour of Lixhe chalk partly saturated by oil and water: experiment and modelling. *Int. J. Numer. Analyt. Methods Geomech.* **26**, No. 9, 897–924.
- Cuccovillo, T. & Coop, M. R. (1999). On the mechanics of structured sands. *Geotechnique* **49**, No. 6, 741–760, <https://doi.org/10.1680/geot.1999.49.6.741>.
- De Gennaro, V., Delage, P., Priol, G., Collin, F. & Cui, Y. J. (2004). On the collapse behaviour of oil reservoir chalk. *Geotechnique* **54**, No. 6, 415–420, <https://doi.org/10.1680/geot.2004.54.6.415>.
- Diambra, A., Ciavaglia, F., Harman, A., Dimelow, C., Carey, J. & Nash, D. F. T. (2014). Performance of cyclic cone penetration tests in chalk. *Geotechnique Lett.* **4**, No. 3, 230–237, <https://doi.org/10.1680/geolett.14.00050>.
- Doughty, L. J., Buckley, R. M. & Jardine, R. J. (2018). Investigating the effect of ageing on the behaviour of chalk putty. In *Engineering in chalk: proceedings of the chalk 2018 conference* (eds J. A. Lawrence, M. Preene, U. L. Lawrence and R. M. Buckley), pp. 549–555. London, UK: ICE Publishing.
- (eds J. A. Lawrence, M. Preene, U. L. Lawrence and R. M. Buckley), pp. 695–701. London, UK: ICE Publishing.
- Fugro (2012). *Onshore geotechnical report: field data St. Nicholas at Wade UK, D34001-1*. Wallingford, UK: Fugro Geoconsulting Ltd.
- Gasparre, A., Nishimura, S., Minh, N. A., Coop, M. R. & Jardine, R. J. (2007). The stiffness of natural London Clay. *Geotechnique* **57**, No. 1, 33–47, <https://doi.org/10.1680/geot.2007.57.1.33>.
- Hancock, J. M. (1975). The petrology of the chalk. *Proc. Geol. Assoc.* **86**, No. 4, 499–535.
- Hickman, R. J. (2004). *Formulation and implementation of a constitutive model for soft rock*. PhD thesis, Virginia Polytechnic Institute and State University, Blacksburg, VA, USA.
- Hobbs, N. B. & Atkinson, M. S. (1993). Compression and tension tests on an open-ended tube pile in chalk. *Ground Engng* **26**, No. 3, 31–34.
- Holloway-Strong, M., Hughes, S. & Hellowell, E. (2007). Stress–deformation behaviour of chalk. *J. Geomech.* **7**, No. 6, 403–409.
- Jardine, R. J. (1992). Some observations on the kinematic nature of soil stiffness. *Soils Found.* **32**, No. 2, 111–124.
- Jardine, R. J., Symes, M. J. & Burland, J. B. (1984). The measurement of soil stiffness in the triaxial apparatus. *Geotechnique* **34**, No. 3, 323–340, <https://doi.org/10.1680/geot.1984.34.3.323>.
- Jardine, R. J., Brooks, N. J. & Smith, P. R. (1985). The use of electrolevel transducers for strain measurements in triaxial tests on weak rock. *Int. J. Rock Mech. Min. Sci. & Geomech. Abstr.* **22**, No. 5, 331–337.
- Jardine, R. J., Buckley, R. M., Kontoe, S., Barbosa, P. & Schroeder, F. C. (2018). Behaviour of piles driven in chalk. In *Engineering in chalk: proceedings of the chalk 2018 conference* (eds J. A. Lawrence, M. Preene, U. L. Lawrence and R. M. Buckley), pp. 33–51. London, UK: ICE Publishing.
- Jardine, R. J., Kontoe, S., Liu, T., Vinck, K., Byrne, B. W., McAdam, R. A., Schranz, F., Andolfsson, T. & Buckley, R. M. (2019). The ALPACA research project to improve design of piles driven in chalk. Improving the design of piles driven in chalk through the ALPACA research project. In *Geotechnical engineering, foundation of the future: proceedings of the XVII ECSMGE-2019* (eds H. Sigursteinsson, S. Erlingsson and B. Bessason), <https://doi.org/10.32075/17ECSMGE-2019-0071>. Reykjavik, Iceland: The Icelandic Geotechnical Society.
- Katsaros, K. I. & Stone, K. J. L. (2018). Long-term stress–strain response of chalk: a micro-mechanical interpretation. In *Engineering in chalk: proceedings of the chalk 2018 conference* (eds J. A. Lawrence, M. Preene, U. L. Lawrence and R. M. Buckley), pp. 687–693. London, UK: ICE Publishing.
- Kohata, Y., Tatsuoka, F., Wang, L., Jiang, G. J., Hoque, E. & Kodaka, T. (1997). Modelling the non-linear deformation properties of stiff geomaterials. *Geotechnique* **47**, No. 3, 563–580, <https://doi.org/10.1680/geot.1997.47.3.563>.
- Korsnes, R., Wersland, E., Austad, T. & Madland, M. (2008). Anisotropy in chalk studied by rock mechanics. *J. Petrol. Sci. Engng* **62**, No. 1, 28–35.
- Kuwano, R. & Jardine, R. J. (2002). On the applicability of cross-anisotropic elasticity to granular materials at very small strains. *Geotechnique* **52**, No. 10, 727–749, <https://doi.org/10.1680/geot.2002.52.10.727>.
- Kuwano, R. & Jardine, R. J. (2007). A triaxial investigation of kinematic yielding in sand. *Geotechnique* **57**, No. 7, 563–579, <https://doi.org/10.1680/geot.2007.57.7.563>.
- Lagioia, R. & Nova, R. (1995). An experimental and theoretical study of the behaviour of a calcarenite in triaxial compression. *Geotechnique* **45**, No. 4, 633–648, <https://doi.org/10.1680/geot.1995.45.4.633>.
- Lawrence, J. A., Mortimore, R. N. & Thrower, A. (2018). Macro and micro fabrics in chalk identified using the bushinsky oil technique: an updated method and new applications for an old experimental technique. In *Engineering in chalk: proceedings of the chalk 2018 conference* (eds J. A. Lawrence, M. Preene, U. L. Lawrence and R. M. Buckley), pp. 549–555. London, UK: ICE Publishing.

- Leddra, M. J., Jones, M. E. & Goldsmith, A. S. (1993). Compaction and shear deformation of a weakly-cemented, high porosity sedimentary rock. In *The engineering geology of weak rock* (eds J. C. Cripps, J. M. Coulthard, M. G. Culshaw, A. Forster, S. R. Hencher and C. F. Moon), pp. 45–54. Rotterdam, the Netherlands: Balkema.
- Leroueil, S. & Vaughan, P. R. (1990). The general and congruent effects of structure in natural soils and weak rocks. *Géotechnique* **40**, No. 3, 467–488, <https://doi.org/10.1680/geot.1990.40.3.467>.
- Lings, M. L., Pennington, D. S. & Nash, D. F. T. (2000). Anisotropic stiffness parameters and their measurement in a stiff natural clay. *Géotechnique* **50**, No. 2, 109–125, <https://doi.org/10.1680/geot.2000.50.2.109>.
- Liu, T. (2018). *Advanced laboratory testing for offshore pile foundations under monotonic and cyclic loading*. PhD thesis, Imperial College, London, UK.
- Liu, T., Ahmadi-Naghadeh, R., Vinck, K., Jardine, R. J., Kontoe, S., Buckley, R. M. & Byrne, B. W. (2022). An experimental investigation into the behaviour of de-structured chalk under cyclic loading. *Géotechnique*, <https://doi.org/10.1680/jgeot.21.00199>.
- Lord, J. A., Clayton, C. R. I. & Mortimore, R. N. (2002). *Engineering in chalk*, C574. London, UK: CIRIA.
- Ma, T., Wei, C., Chen, P. & Li, W. (2019). Chemo-mechanical coupling constitutive model for chalk considering chalk–fluid physicochemical interaction. *Géotechnique* **69**, No. 4, 308–319, <https://doi.org/10.1680/jgeot.17.P115>.
- Marley, S. (2020). *Correlation of the lithostratigraphic and geomechanical properties of the chalk rock in the transitional zone province*. MSc dissertation, Imperial College, London, UK.
- Matthews, M. C. & Clayton, C. R. I. (1993). Influence of intact porosity on the engineering properties of a weak rock. In *Proceedings of the 1st international symposium on geotechnical engineering of hard soils–soft rocks* (eds A. Anagnostopoulos, F. Schosser, N. Kalteziotis and R. Frank), pp. 693–702. Rotterdam, the Netherlands: Balkema.
- Mesri, G. & Vardhanabhuti, B. (2006). Discussion of ‘Secondary compression’. *J. Geotech. Geoenviron. Engng* **132**, No. 6, 817–818.
- Mortimore, R. N. (2012). The 11th Glossop Lecture: making sense of chalk: a total-rock approach to its engineering geology. *Q. J. Engng Geol. Hydrogeol.* **45**, No. 3, 252–334.
- Muir Wood, A., Mackenzie, B., Burbury, D., Rattley, M., Clayton, C. R. I., Mygind, M., Wessel Andersen, K., Le Blanc Thilsted, C. & Albjerg Liingaard, M. (2015). Design of large diameter monopiles in chalk at Westernmost Rough offshore wind farm. In *Frontiers in offshore geotechnics III* (ed. V. Meyer), pp. 723–728. Leiden, the Netherlands: CRC Press/Balkema.
- Nash, D. F. T., Sills, G. C. & Davison, L. R. (1992). One-dimensional consolidation testing of soft clay from Bothkennar. *Géotechnique* **42**, No. 2, 241–256, <https://doi.org/10.1680/geot.1992.42.2.241>.
- Pedone, G., Kontoe, S., Zdravkovic, L. & Jardine, R. J. (2020). *Supergen ORE flexible funding research project ALPHA: numerical analysis of laterally loaded piles driven in chalk, final report*. London, UK: Imperial College.
- Petley, D., Jones, M. E., Fan, C., Stafford, C., Leddra, M. J. & Kågeson-Loe, N. (1993). Deformation and fabric changes in weak fine-grained rocks during high pressure consolidation and shear. In *Proceedings of the 1st international symposium on geotechnical engineering of hard soils–soft rocks* (eds A. Anagnostopoulos, F. Schosser, N. Kalteziotis and R. Frank), pp. 737–743. Rotterdam, the Netherlands: Balkema.
- Razoaki, R. N. (2000). *Effect of ageing on mechanics of chalk slurries*. PhD thesis, University of Portsmouth, Portsmouth, UK.
- Røgen, B., Fabricius, I. L., Japsen, P., Høier, C., Mavko, G. & Pedersen, J. M. (2005). Ultrasonic velocities of North Sea chalk samples: influence of porosity, fluid content and texture. *Geophys. Prospect.* **53**, No. 4, 481–496.
- SETech (2007). *Trial site investigation – Thanet offshore wind farm trial site*, 8564/1. North Shields, UK: SETech (Geotechnical Engineers) Ltd.
- Skempton, A. W. (1954). The pore-pressure coefficients *A* and *B*. *Géotechnique* **4**, No. 4, 143–147, <https://doi.org/10.1680/geot.1954.4.4.143>.
- Taibi, S., Duperret, A. & Fleureau, J. M. (2009). The effect of suction on the hydro-mechanical behaviour of chalk rocks. *Engng Geol.* **106**, No. 1-2, 40–50.
- Talesnick, M. L., Hatzor, Y. H. & Tsesarsky, M. (2001). The elastic deformability and strength of a high porosity, anisotropic chalk. *Int. J. Rock Mech. Min. Sci. & Geomech. Abstr.* **38**, No. 4, 543–555.
- Tatsuoka, F., Jardine, R. J., Lo Presti, D., Di Benedetto, H. & Kodaka, T. (1999). Theme lecture: characterising the pre-failure deformation properties of geomaterials. In *Proceedings of the 14th international conference on soil mechanics and foundation engineering*, pp. 2129–2164. Rotterdam, the Netherlands: Balkema.
- Vinck, K. (2021). *Advanced geotechnical characterisation to support driven pile design at chalk sites*. PhD thesis, Imperial College London, London, UK.
- Whittle, R., Palix, E. & Donaghy, D. (2017). The influence of insertion process on determining the stiffness characteristics of chalk, using Pre-bored, self-bored and pushed pressuremeters. In *Proceedings of the 8th international conference on offshore site investigation and geotechnics: smarter solutions for offshore developments*, vol. 1, pp. 308–315. London, UK: Society for Underwater Technology.
- Withers, N. J., Howie, J., Hughes, J. M. O. & Robertson, P. K. (1989). Performance and analysis of cone pressuremeter tests in sands. *Géotechnique* **39**, No. 3, 433–454, <https://doi.org/10.1680/geot.1989.39.3.433>.